AFCRL-71-0537
Report MDC Q0464
September 1971
Copy No. III

740901

A Multiphasic Investigation of an Argon Plasma in a rf Discharge and Sonic Afterglow

Louis N. Medgyesi-Mitschang and Ray A. Hefferlin
McDonnell Douglas Research Laboratories
McDonnell Douglas Corporation, St. Louis, Missouri 63166

Contract No. F19628-71-C-0024
Project No. 4642
Task No. 464203
Work Unit No. 46420301

Scientific Report No. 1

Sheldon B. Herskovitz, Contract Monitor
Microwave Physics Laboratory

Approved for Public Release; Distribution Unlimited

Prepared for

AIR FORCE CAMBRIDGE RESEARCH LABORATORIES
AIR FORCE SYSTEMS COMMAND
UNITED STATES AIR FORCE
BEDFORD, MASSACHUSETTS 01730

MCDONNELL DOUGLAS

Unclassified

Security Classification

DOCUMENT CONTROL DATA - R & D

(Security classification of title, body of abstract and indexing annotation must be entered when the overall report is classified)

1 ORIGINATING ACTIVITY (Corporate author)	2a. REPORT SECURITY CLASSIFICATION
McDonnell Douglas Research Laboratories McDonnell Douglas Corporation St. Louis, Missouri 63166	NONE 2b GROUP

3 REPORT TITLE

A MULTIPHASIC INVESTIGATION OF AN ARGON PLASMA IN A RF DISCHARGE AND SONIC AFTERGLOW

4 DESCRIPTIVE NOTES (Type of report and inclusive dates)

Scientific Interim

5 AUTHOR(S) (First name, middle initial, last name)

Louis N. Medgyesi-Mitschang
Ray A. Hefferlin

6 REPORT DATE	7a. TOTAL NO OF PAGES	7b NO OF REFS
September 1971	41	31

8a CONTRACT OR GRANT NO	9a. ORIGINATOR'S REPORT NUMBER(S)
F19628-71-C-0024 b PROJECT, TASK, WORK UNIT NOS 4642-03-01 c. DoD Element 62101F d DoD Subelement 684642	Scientific Report No. 1 9b OTHER REPORT NO(S) (Any other numbers that may be assigned this report) AFCRL-71-0537, MDC Q0461

10 DISTRIBUTION STATEMENT

A - Approved for public release; distribution unlimited

11 SUPPLEMENTARY NOTES	12 SPONSORING MILITARY ACTIVITY
TECH, OTHER	Air Force Cambridge Research Laboratories (LZ) L G Hanscom Field Bedford, Massachusetts 01730

13 ABSTRACT

Microwave interferometric and radiometric, optical spectrometric and thermocouple measurements of the electron density and the electron, the excitation, and the gas temperatures have been made in the active discharge and sonic afterglow of an argon plasma generated by a rf generator. The optical measurements were made in the 4000–5000 Å region for discharge pressures of 60–650 Torr. Excitation temperatures in the discharge ranged between ~7000–10,000K The electron temperatures from the radiometer measurements were compared with the excitation temperatures. Thermocouple measurements, gas dynamic calculations and rotational spectra from traces of N_2 injected in the argon indicated that the gas temperatures in the discharge and the afterglow were 2900–4400K and 1900–3300K, respectively, indicating a two-temperature state in both regions. Results of this investigation indicated local thermodynamic equilibrium (LTE) for all excited levels

DD FORM 1 NOV 65 1473 (PAGE 1)

S/N 0101-807-6801

Unclassified

Security Classification

Unclassified

Security Classification

14 KEY WORDS	LINK A		LINK B		LINK C	
	ROLE	WT	ROLE	WT	ROLE	WT
Plasma diagnostics						
rf Plasma						
Optical spectroscopy						
Microwave Radiometry						

DD FORM 1 NOV 65 1473 (BACK)

(PAGE 2)

Unclassified

Security Classification

A Multiphasic Investigation of an Argon Plasma in a rf Discharge and Sonic Afterglow

Louis N. Medgyesi-Mitschang and Ray A. Hefferlin*

McDonnell Douglas Research Laboratories

McDonnell Douglas Corporation, St. Louis, Missouri 63166

Abstract

Microwave interferometric and radiometric, optical spectrometric and thermocouple measurements of the electron density and the electron, the excitation, and the gas temperatures have been made in the active discharge and sonic afterglow of an argon plasma generated by a rf generator. The optical measurements were made in the 4000-5000 Å region for discharge pressures of 60-650 Torr. Excitation temperatures in the discharge ranged between ~7000-10,000 K. The electron temperatures from the radiometer measurements were compared with the excitation temperatures. Thermocouple measurements, gas dynamic calculations and rotational spectra from traces of N_2 injected in the argon indicated that the gas temperatures in the discharge and the afterglow were 2900-4400 K and 1900-3300 K, respectively, indicating a two-temperature state in both regions. Results of this investigation indicated local thermodynamic equilibrium (LTE) for all excited levels.

Consultant, Permanent address: Southern Missionary College, Collegedale, Tenn. 37315

Table of Contents

This document consists of
a title page, pages i and iii
and pages 1 through 36.

1 Introduction and background

The processes which govern the production and loss of electrons together with reactions between ions and neutrals play an important role in determining the plasma environment of a vehicle during planetary reentry. In many instances it would be desirable to be able to control the composition of this plasma. To accomplish this objective, it is necessary to know what are the dominant reaction processes and reaction rates at temperatures encountered during reentry (2000-4000 K). Also of interest are the chemical reactions which occur when target gas molecules interact with a plasma in this high temperature range.

Reactions associated with plasma, at elevated temperatures ($\geq$ 1000 K) exhibit significantly different behavior than the analogous reactions occurring at room temperature. The specific reaction pathways, and rate constants of these reactions are of special interest at these temperatures.[1,2]

An experimental system has been developed at McDonnell Douglas Research Laboratories that permits investigation of high temperature plasma reactions over a broad range of plasma conditions.[3] At present, only electron attachment reactions are being investigated because of the wide interest in electrophilic molecules. A sonic afterglow serves as a chemical reaction region for interactions between the neutral electrophilic molecules and the plasma. The state of the plasma is monitored by a variety of diagnostic techniques in both the discharge and afterglow regions. The results of optical spectrometer, microwave radiometer, microwave interferometer measurements, as well as supplementary thermocouple data and gas temperature calculation, presented in this paper allow accurate characterization of the conditions in the discharge and afterglow regions. Knowledge of these conditions is essential for the interpretation of the chemical kinetics involved in the reaction between the plasma and the injected electrophilic molecules.

In the past, many techniques have been developed to determine the important plasma parameters such as the electron temperature, excitation temperature, and electron density. Most prominent of these have been Langmuir probes and optical spectrometric methods. Spectrometric, radiometric, and interferometric techniques have the advantage of allowing plasma diagnosis without introducing perturbations into the gas. Early experiments by Knol[4], and Easley and Munford[5] have demonstrated that the radiometrically determined electron temperatures compared favorably with those obtained from Langmuir probe measurements in low pressure Hg-Ar discharges. More recently, McGregor and Brewer[6] have found that in certain cases the spectrometrically measured excitation temperatures correlate with the electron temperatures measured with Langmuir probes in an argon plasma jet. Similar correlation of the radiometric temperature data with spectrometric results was found by Dellis[7] and Harding et al.[8]

In this report the excitation temperature measured by a spectrometer and the electron temperature obtained from a radiometer are compared.

Electron densities obtained from spectrometric measurements in the sonic afte glow channel are compared with interferometrically measured values extrapolated into the channel from the free jet. The calculated gas (heavy particle) temperatures obtained from gas dynamic considerations both in the channel and the discharge chamber and from molecular rotational lines in the channel, are compared with thermocouple data obtained in the afterglow channel for various levels of input rf power. These measurements are used to examine the existence of local thermodynamic equilibrium (LTE) in the active discharge region and the sonic afterglow.

LTE is expected to hold if collisional processes involving a Maxwellian electron distribution dominate the rate equations governing the population of a given quantum level. A "critical level" may be defined at which the collisional excitation rates are comparable to or exceed the radiative decay rates. The (electron) temperature associated with the energy distribution of free electrons can be assumed to be in equilibrium with the (excitation) temperature of states whose levels are above the critical level.

If LTE is established above a certain level, the population in the various levels above this level can be related with each other via the Boltzmann distribution. In addition, if it can be shown that the plasma is optically thick, reabsorption of radiation can occur, resulting in an effective reduction of the radiative decay rates so that LTE can exist at some lower level than that at which radiation and collisional processes are comparable. However, as will be noted later, the plasma in both the active discharge and the sonic afterglow (reaction channel) regions is optically thin. Conditions mitigating against unqualified LTE are time variations in the discharge, spatial gradients in the electron density, and strong electromagnetic fields.

2 Experimental apparatus

The apparatus associated with this experiment is shown in Fig. 1. It has been described in considerable detail elsewhere.[3] Only those elements of the system which have a direct bearing upon the spectrometric and microwave measurements will be described here. The experimental apparatus germane to this discussion consists of the plasma source followed by the reaction channel, the spectrometer and ancillary optical system, and the microwave radiometer and microwave interferometer.

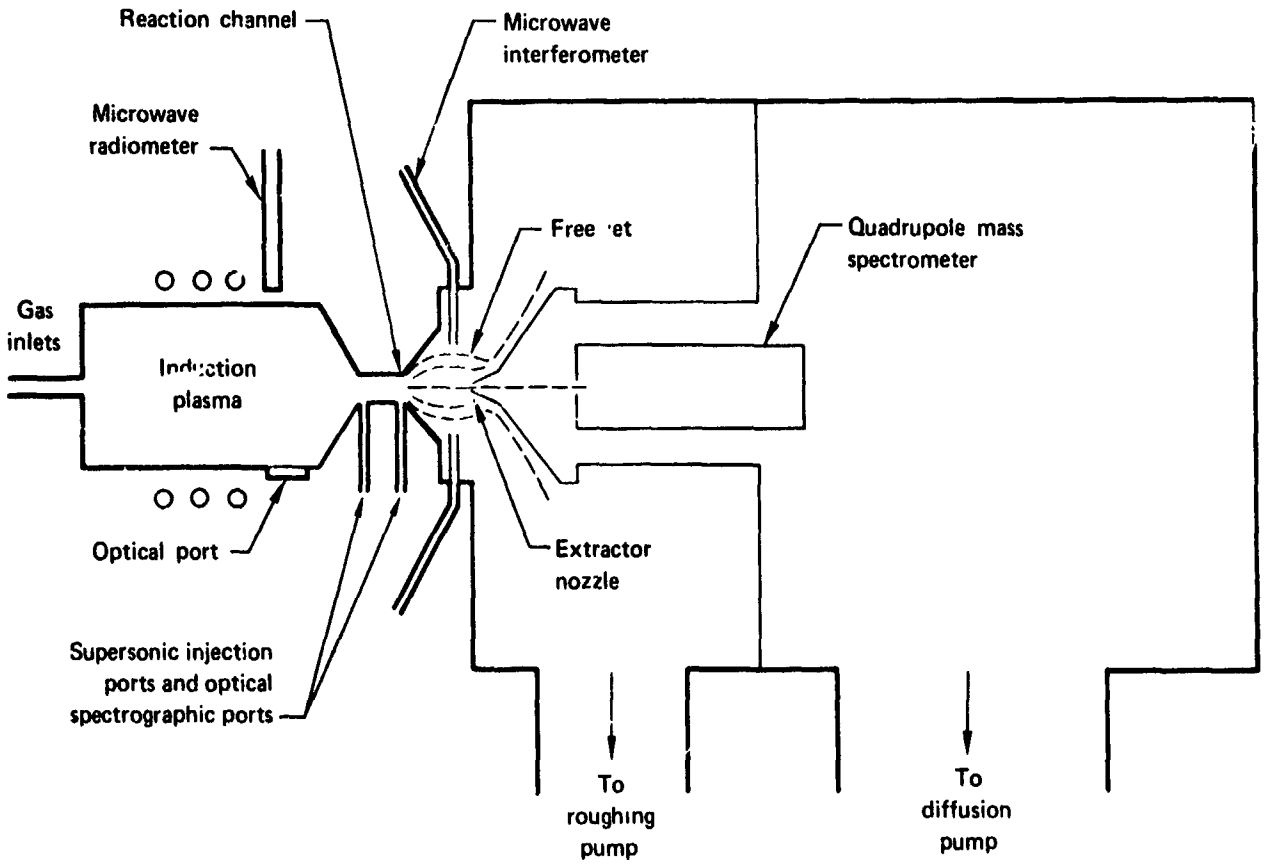

Fig. 1 Experimental apparatus for high temperature plasma reaction studies (Mullen et al., Rev. Sci. Instr. 41, 1746 (1970))

For the source, an electrodeless induction argon plasma similar to that of Reed[9] and Eckert el al.[10], is used. This source is free of electrode contamination making it particularly suitable for high temperature chemistry studies. The plasma generator is a 100 kW, class C, rf oscillator operating at 540 kHz. The power input to the rf oscillator can be varied continuously from 0 to 100 kW. For the measurements described in this paper input rf power levels of 42, 48, 54, and 60 kW were chosen. The following variables are monitored: oscillator plate, grid, tank voltages and currents, input power per phase, grid coupling, feedback control and rf frequency. The temperature rise in the rf coil cooling water, the chamber pressure and the input mass flow rate are also monitored. Any generator operating condition can be reset to ±5% duplicating previously obtained conditions.

The discharge tube is made of 1 mm thick quartz, 80 mm in diam 160 mm long, and is sandwiched between O-ringed, water-cooled copper end plates. The relative physical dimensions of the discharge chamber itself are indicated in Fig. 2. The discharge gas inlets pass through one of the copper end plates. Typical argon mass flow rates are 0.10 to 0.36 g/sec as shown in Fig. 3. The rf power is coupled through two eight-turn counterwound coils of 3 mm o.d. copper tubing that surround the plasma tube. The coils are center fed for minimum rf plasma potential at each end of the discharge.[11] A 1.5 mm clearance between the discharge tube and a Teflon water jacket allows adequate coolant water flow. The partially ionized argon is passed from the discharge chamber into a 4 mm diam sonic reaction channel, and then expanded as a free jet into a large vacuum tank at 0.2 Torr pressure.

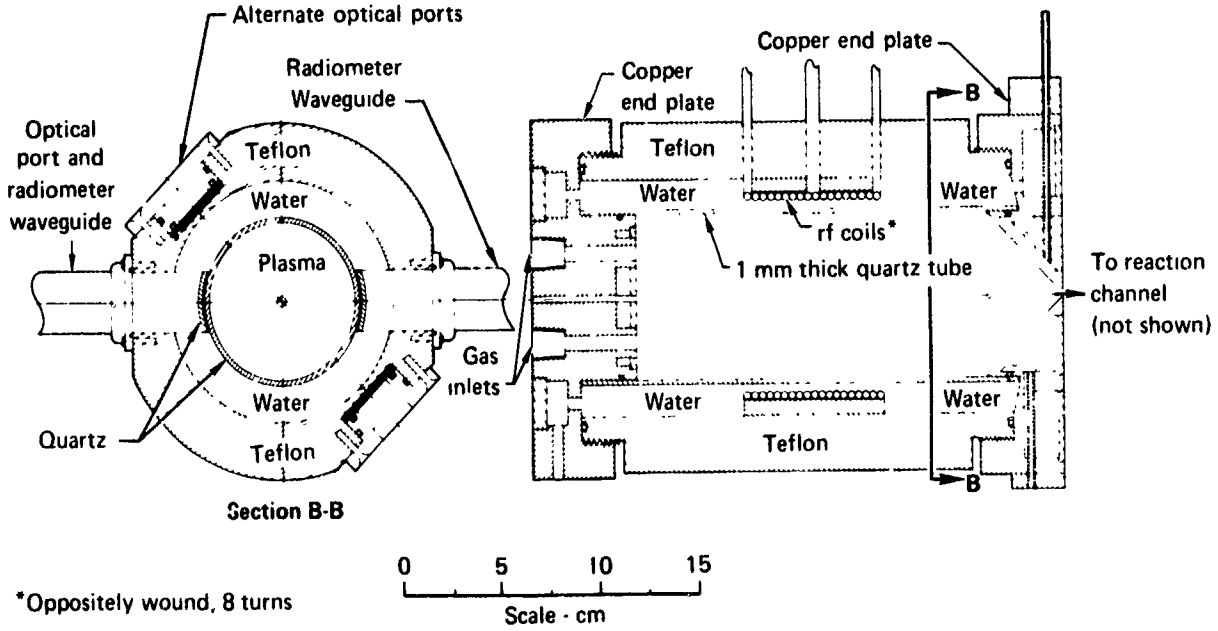

Fig. 2 Discharge chamber and arrangement of rf excitation coils (Mullen et al., Rev. Sci. Instr. 41, 1746 (1970))

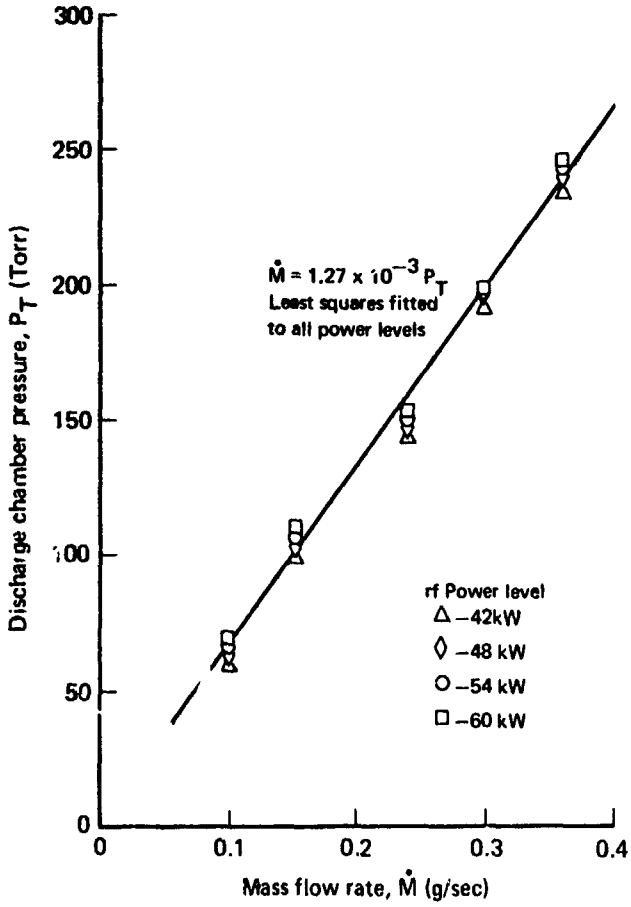

Fig. 3 Measured mass flow rates in discharge chamber

2.1 Optical instrumentation

Spectroscopic determination of the argon excitation temperature and the electron density in the discharge chamber and the reaction channel was made using the optical arrangement outlined in Fig. 4. A 1 m (Jarrell-Ash Model 78-466) Czerny-Turner scanning spectrometer was used in these experiments. The plasma radiation from the discharge chamber was transferred to the spectrometer using a 0.32 cm diam by 14.1 cm long fiber bundle, with plane-polished ends. The bundle was mounted in the radiometer port with its input end flush against the quartz window. Then, a lens was used to form an image of the end of the bundle on the spectrometer slit. A similar arrangement with an aluminized quartz rod was tried and found to be less satisfactory due to the fragility of the aluminum coating. A photomultiplier tube was used with the resulting output displayed by a strip chart recorder (modified Honeywell Electronic 16).

A plane window standard 35A tungsten lamp was used for calibration of the optical system. The entire measurement system from the fiber bundle onward, was removed from the discharge chamber and the light from the lamp was transferred to the input of the fiber bundle. Spectrum scans were obtained in the 4000-5000 Å region. A filter was used to eliminate second-order features.

Spectroscopic measurements in the discharge were made for a range of discharge pressures of 60-650 Torr and input power levels of 42-60 kW. The spectrum scans were obtained over the entire pressure range by adjusting the mass flow rate to the discharge chamber, holding the input power constant. Usually the spectrum scans were made for increasing chamber pressures, followed by scans retracing the pressure range. In this way the repeatability of the data could be checked. During data acquisition, the rf generator was operated uninterrupted for long periods (often exceeding one hour). During these long periods of operation the generator was found to be stable and showed no perceptible drift in its operating characteristics. The special anti-sputtering design of the rf coil and the optimized configuration of the discharge chamber prevented contamination of the plasma.

For the optical measurements in the reaction channel, the fiber bundle light pipes were integrally bonded to the reaction channel. Their mounting was flush with the inside wall of the channel, causing no perturbation in the plasma stream. Light intensities observed were substantially weaker than those from the discharge chamber and care was taken to align the spectrometer via a small laser. Again, spectrum scans were made for the previously noted range of rf power and discharge chamber pressures.

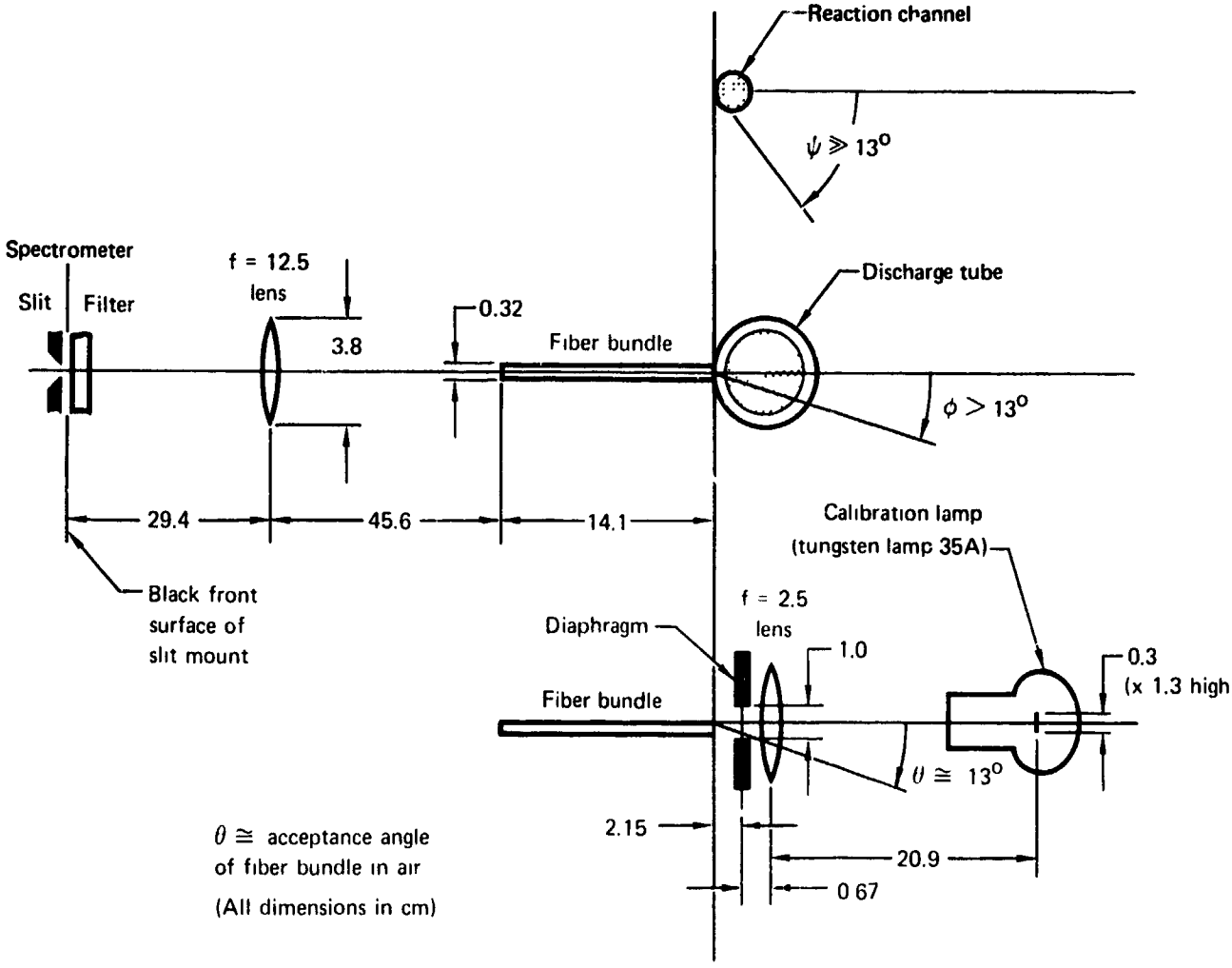

Fig. 4 Arrangement of optics for spectrometric measurements

2.2 Radiometer and associated instrumentation

For the radiometric measurements a modified Dicke X-band microwave radiometer operating at 8.5 GHz center frequency was used.[12-15] The basic radiometer circuit is shown in block diagram form in Fig. 5. In operation the radiometer was electronically switched between the plasma and a standard waveguide noise source consisting of an argon-filled tube mounted obliquely to the E-plane in a rectangular waveguide. The standard source presents a low VSWR, less than 1.2, with or without an argon plasma present in the above tube. Spurious electromagnetic modes due to the presence of the gas tube are suppressed within the waveguide. With the gas tube on, the white noise spectrum is generated over the bandwidth of the waveguide. For radiometric measurements, the gas tube was operated in the cw mode. The standard noise source, together with a 50 dB precision attenuator formed a calibrated blackbody temperature standard with equivalent temperature $> 10{,}000$ K. Due to the low plasma emissivity, the effective thermal radiation from the plasma corresponded to a substantially lower temperature.

The signal from the plasma and the standard are alternately gated into the radiometer by a crystal switch. The two signals are detected, amplified, and processed by passing them through a balanced low noise mixer i.f.-pre-amp combination followed by a high gain i.f. amplifier and a coherent detector synchronized with the crystal switch, as shown in Fig. 5. The output is detected on a precision microvoltmeter.

To assure symmetry in operation, test signals were fed to ports A and B of the crystal switch, alternately switched and compared. Slight discrepancies between the two ports were corrected by adjusting the E-H tuning plungers in the switch. Balanced operation was verified by connecting identical noise sources to the input ports of the switch and observing a null on the radiometer output.

The radiometer receiving antenna is a contoured open-ended waveguide, capped by a similarly contoured 1.5 mm thick quartz window. The waveguide is oriented so that the E-plane is parallel to the axis of the discharge chamber, resulting in the minimum mismatch. The alternate polarization proved less satisfactory for coupling. Contouring the waveguide to the curvature of the discharge tube minimized the necessary water gap between the antenna and the discharge jacket, thus limiting the absorption in the water film to 1 dB. The above optimum arrangement satisfied the dual requirements of close coupling of the antenna to the plasma and proper cooling of both antenna window and discharge tube.

Initially with the discharge off, the radiometer antenna with an E-H tuner was connected to the discharge chamber using a coherent test signal at the center frequency of the radiometer. An isolator was inserted to maintain a low VSWR in the antenna leg with changing plasma conditions and to prevent any local oscillator leakage. Upon switching to the radiometer mode, a signal corresponding to a 300 K blackbody source was measured. With the plasma on, the thermal radiation from the plasma was measured radiometrically at a generator input power of 54 kW, representing the mid-range of input power. In these measurements the pressure in the discharge chamber was varied by changing the mass flow rate in the chamber. The rf power was maintained constant. The readings were obtained by setting the precision attenuator for a null output. The average of three consecutive readings was taken at each pressure setting and the result recorded. After sweeping through the pressure range, as with the optical measurements, the pressure range was retraced and the data were compared with previously obtained values for repeatability. Suitable cooling of the discharge chamber allowed all the microwave components in close proximity with the discharge to remain at a constant ambient temperature during the experiment. After a sweep plus retrace of the pressure range, the discharge was extinguished and the radiometer nulled with the precision attenuator. The attenuator setting was compared with the initial value at the beginning of the experiment, thereby serving as an index of drift stability. Because of the good drift compensation characteristics of the mixer and i.f. stages, negligible drift was noted when the microwave circuit was properly tuned.

To obtain an electron temperature from the radiometer measurements, the plasma emissivity was determined. A plane wave analysis compatible with the physical dimensions of the radiometer antenna and the diameter of the plasma discharge (8 cm in diam) was used. Incoherence in the power reflectance inside the plasma was assumed. Separate reflectance and transmission measurements were made in the discharge at various chamber pressures. The plasma induced attenuation was shown to exceed 50 dB. Using these considerations, the expression for the plasma emissivity was computed as a function of the total pressure in the discharge, the gas temperature, the measured mass flow in the chamber, and the electron density. The analysis included the effect of both Coulomb and electron-neutral interactions. The main points of this analysis are summarized in Appendix A.

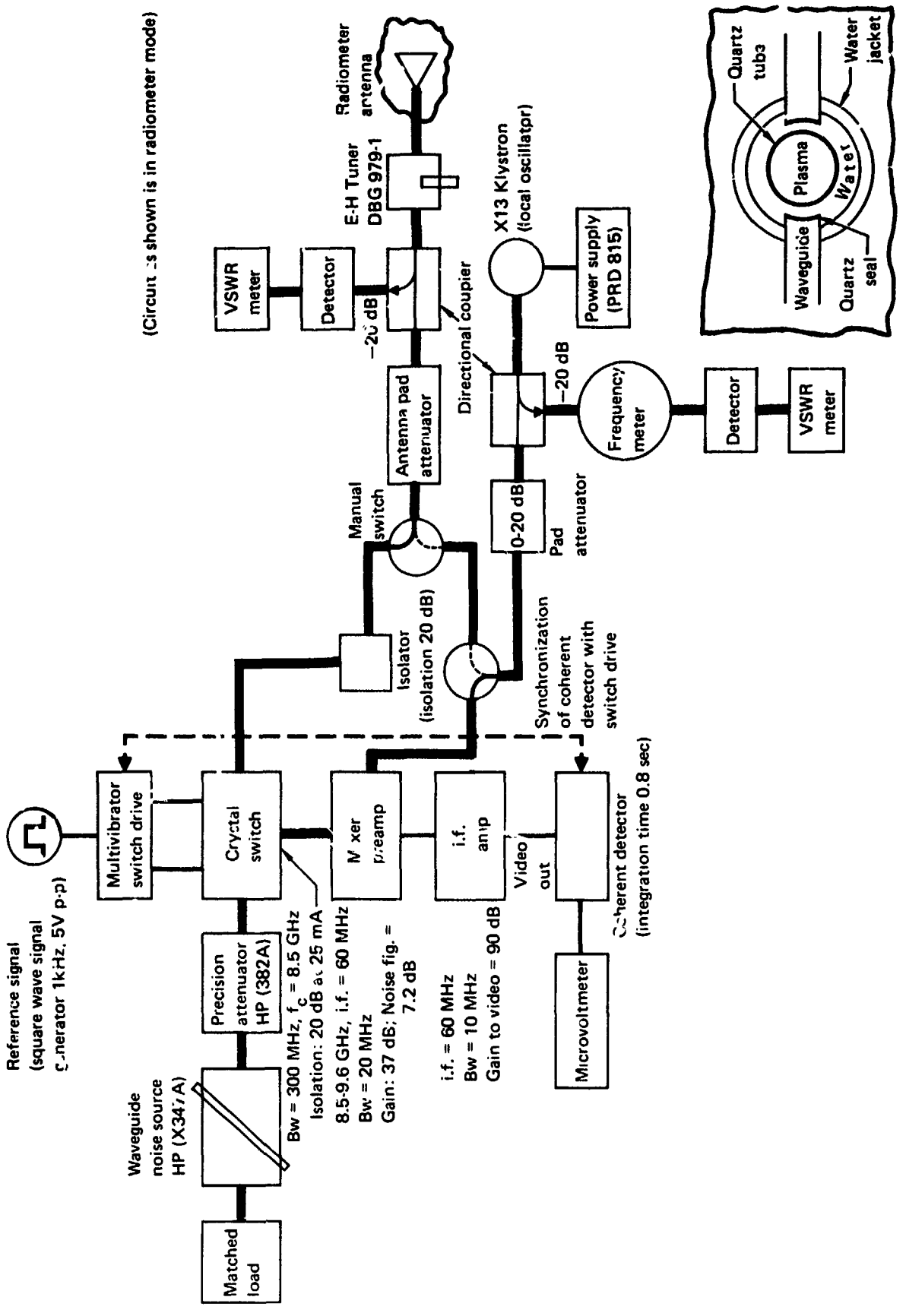

Fig. 5 Radiometer schematic
(Mullen et al., Rev. Sci. Instr. 41, 1743 (1970))

2.3 Microwave interferometer

Electron densities were measured in the free jet region, 3.58 cm downstream from the exit plane of the reaction channel using a microwave interferometer as shown in Fig. 6. Open ended wave guides (E plane polarized perpendicular to the channel axis) used for antennas are located so that the plasma is just outside of the antenna near field. To prevent reflections in the plasma leg of the interferometer from entering the circuit, an isolator is used behind the transmitting antenna. Similarly, another isolator is placed behind the receiving antenna so that the crystal detector can be tuned to the incident signal only, avoiding reactance tuning due to the plasma path length. Precision phase shifters and attenuators are used throughout the circuit to obtain maximum accuracy.

With the plasma off, the interferometer is null adjusted using the precision attenuators and phase shifters. With the plasma on, the path propagation characteristics between the antennas is altered and the interferometer is renulled. The plasma by-pass arm in the circuit permitted the interferometer to be nulled during the experiment, thereby checking drift. Because the plasma is underdense at the exit plane where the interferometer is situated (Fig. 1), the electron-ion collision frequency ν is small compared to the interferometer signal frequency f (i.e., $\lesssim 10^{-3}$). No appreciable plasma attenuation is observed and the electron density may be determined from phase shift measurements alone, using a collisionless plasma model with a parabolic profile.

Assuming that isentropic expansion occurs past the exit plane of the reaction channel, the electron density was shown to be approximately a factor of 354 higher in the channel than that measured 3.58 cm further downstream.[3] The electron densities were measured over the range of conditions paralleling those for the optical measurements.

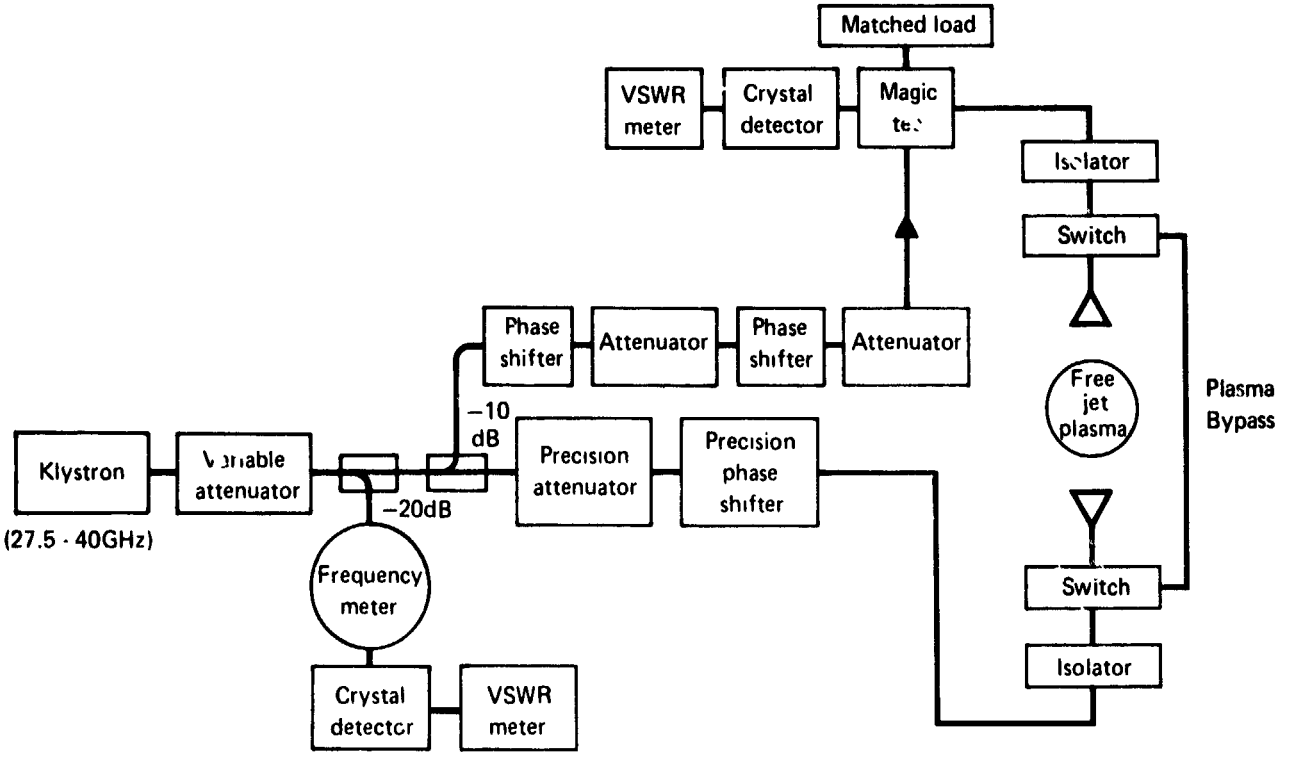

Fig. 6 Ka-band microwave interferometer block diagram

3 Summary of measurements

3.1 Optical measurements

For the chamber pressures investigated the optical data contained no visible ArII lines in the spectra. The ArI were in no case wider than the instrument resolution width (1.2 Å). This observation allowed placing an order of magnitude upper limit of 10^{16} e/cm on the electron density. For excitation temperature determination, the following ArI lines were selected: 4158.6 Å, 4164.2 Å, 4181.9Å, 4259.4 Å, 4266.3 Å, 4272.2 Å, 4300.1 Å, 4345.2 Å, and 4510.7 Å. Boltzmann plots were obtained from the measured line intensities. From these the excitation temperatures were obtained by least squares fitting to the Boltzmann relationship describing the intensity of a spectral line,

$$\log_{10} \frac{I\lambda^3}{gf_{nm}} = \log_{10} \left[\frac{2\pi\, he^2}{mU}\right] N_o - \frac{5040}{T_{exc}} E_n$$

where h = Planck's constant,
g = statistical weight,
f_{nm} = emission oscillator strength,
U = atom partition function,
N_o = total number of atoms per cm^3,
λ = wavelength of emitted ratiation,
I = intensity of atomic spectral line (ergs sec^{-1} $ster^{-1}$ cm^{-2}),
E_n = excitation energy of level n (eV), and
T_{exc} = excitation temperature.

In using this relationship two assemptions were implicit: 1) The plasma was assumed to be optically thin in the wavelength region scanned so that self-absorption was absent and 2) the excited states were assumed to possess a Boltzmann distribution.

The plasma was shown to be optically thin and thus no self-absorption was present since the measured spectral radiances of the ArI lines were not comparable to the values predicted by the Planck function. For example, the peak measured spectral radiances were 10^{11} –10^{13} ergs sec^{-1} $ster^{-1}$ cm^{-3}. The Planck function at the same wavelengths predicts ~ 2 x 10^{15} ergs sec^{-1} $ster^{-1}$ cm^{-3} for T = 9000 K in the discharge and ~1 x 10^{14} ergs sec^{-1} $ster^{-1}$ cm^{-3} for T = 5000 K in the reaction channel.

The excitation temperatures in the discharge chamber and the reaction channel are summarized in Tables 1 and 2. Figure 7 shows a typical Boltzmann plot for the data obtained in the reaction channel.

The electron density was calculated from the continuum radiation via the recently corrected Kramers-Unsöld equation.[16] This formulation states that the spectral radiance of the continuum of an LTE argon plasma at an electron temperature T_e (and with a calculable electron density, N_e) is

$$\epsilon_\nu = (5.443) \times 10^{-39} N_e^2 T_e^{-1/2}$$

ergs sec^{-1} $ster^{-1}$ cm^{-3} Hz.

Table 1 Representative spectrometric results for discharge chamber

Chamber pressure (Torr)	Power (kW)	T_{exc} (K)	N_e (e/cm^3)	Chamber pressure (Torr)	Power (kW)	T_{exc} (K)	N_e (e/cm^3)
75	42	9924	8.5×10^{15}	63	54	10218	1.17×10^{16}
100	42	9777	8.68×10^{15}	100	54	9351	1.17×10^{16}
				127	54	9613	1.16×10^{16}
125	42	8778	8.40×10^{15}	150	54	9435	1.02×10^{16}
				180	54	9154	1.17×10^{16}
150	42	8062	8.22×10^{15}	202	54	7684	0.925×10^{16}
				252	54	7592	1.14×10^{16}
175	42	6446	7.45×10^{15}	305	54	6360	1.18×10^{16}
200	42	8234	7.7×10^{15}	353	54	8172	1.34×10^{16}
250	42	8555	8.63×10^{15}	417	54	9253	1.43×10^{16}
300	42	7398	9.74×10^{15}	475	54	8223	1.46×10^{16}
350	42	8729	1.0×10^{16}	535	54	7352	1.48×10^{16}
425	42	8631	1.23×10^{16}	644	54	8722	1.51×10^{16}
				100	60	9729	1.19×10^{16}
75	48	13709	1.1×10^{16}	150	60	8823	1.07×10^{16}
100	48	9853	1.04×10^{16}	200	60	6719	1.1×10^{16}
150	48	6898	8.9×10^{15}	250	60	6064	1.22×10^{16}
200	48	8389	1.4×10^{16}	300	60	7914	1.27×10^{16}
250	48	7884	1.0×10^{16}				
300	48	7286	1.09×10^{16}				
350	48	6723	1.18×10^{16}				
425	48	8612	1.33×10^{16}				
525	48	7383	1.37×10^{16}				

Table 2 Representative spectrometric results for reaction channel

Chamber pressure (Torr)	Power (kW)	T_{exc} (K)	N_e (e/cm^3)	Chamber pressure (Torr)	Power (kW)	T_{exc} (K)	N_e (e/cm^3)
113	42	6462	1.06×10^{15}	100	54	6066	0.98×10^{15}
145	42	4962	1.09×10^{15}	125	54	5746	1.08×10^{15}
177	42	7811	1.43×10^{15}	150	54	5211	1.2×10^{15}
203	42	4408	1.36×10^{15}	200	54	5340	1.23×10^{15}
233	42	5224	1.55×10^{15}	200	54	5178	1.3×10^{15}
267	42	4929	1.66×10^{15}	225	54	4481	1.17×10^{15}
300	42	4568	1.7×10^{15}	250	54	5682	1.38×10^{15}
				275	54	4673	1.56×10^{15}
				300	54	4356	1.74×10^{15}
125	48	5625	0.97×10^{15}	325	54	4943	1.70×10^{15}
150	48	5360	1.1×10^{15}				
175	48	5339	1.25×10^{15}	81	60	4912	0.93×10^{15}
200	48	5818	1.37×10^{15}	112	60	4905	0.99×10^{15}
250	48	5666	1.56×10^{15}	144	60	3936	1.0×10^{15}
300	48	4884	1.56×10^{15}	174	60	4768	1.22×10^{15}
				200	60	4757	1.27×10^{15}
				230	60	4702	1.15×10^{15}
				263	60	3600	1.1×10^{15}

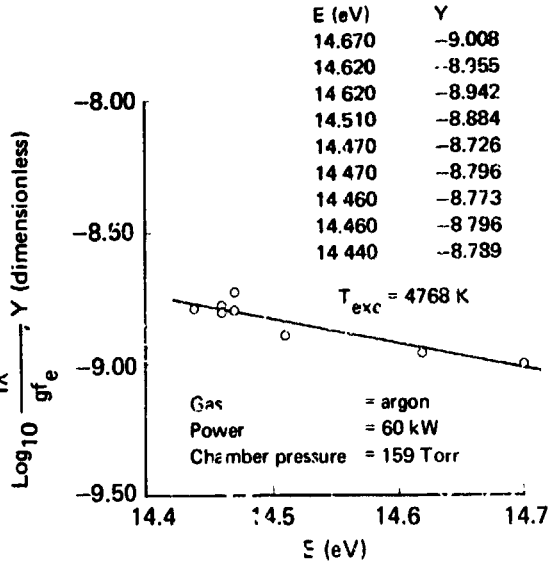

Fig. 7 Boltzmann plot for excitation temperatures in reaction channel

The empirical constant in this equation is taken from Richter[17] and Olsen[18]. The continuum measurements, taken at $\lambda = 4500$ Å, were uninverted, that is, the source was not traversed. Data taken for different slit widths agreed. The oscillator strengths used in the data reduction are given in the recent NBS critical compilation of measured oscillator strengths.[19]

The electron densities in the discharge chamber, using the Kramers-Unsöld equation, are given in Fig. 8. These values assume the effective depth of the plasma to be 2 cm. The measured densities vary by a factor of two (0.70 to 1.4 x 10^{16} e/cm^3) over the pressure range from 40 to 540 Torr at the lower rf power levels (42 and 48 kW), but remain a relatively constant function of discharge pressure at 60 kW. Similar values were measured by Hughes and Wooding[20] and Goldfarb and Dresvin[21] for

Table 3 Comparison of argon rf plasma sources

Investigator	rf power (kW)	Coil turns	Freq (MHz)	Mass flow rate (g/sec)	Discharge dia. (mm)	Pressure (Torr)	Peak N_e (e/cm^3)	Method	Peak T_e (K)	Method	T_{exc} (K)	Method	Average T_g (K)	Method	Profile
V M Goldfarb, S.V Dr zvin High Temp (Russ.) 3, 303 (1965)	2 3*	3	26	7 4 10 4 x 10^{-2}	16	760	1 2 x 10^{16}	Photog. of cont.	$T_g = T_{exc} = T_e$		9750	Photog. of cont.	9500	Abs. Intens. Ar I at 4510 Å	Radial
				6 18 x 10^{-2}	22	760	1 15 x 10^{16}	Abs. Intens. Ar cont	$T_g = T_{exc} = T_e$		9700	Abs. Intens. Ar cont.	9400	Broadening of H_β lines	Radial
				3 6 - 5 4 x 10^{-1}	30	760	0 88 x 10^{16}	Photog of cont	$T_g = T_{exc} = T_e$		9500	Photog. of cont.	9100	Abs. Intens. Ar I at 4510 Å	Radial
P D Johnson, Phys Letters 20, 499 (1966)	6	5	4 5		51	760	4 4 x 10^{15}	Stark and broadening	9700	Olsen correction factor used	9000±500	Saha Eq			Radial
D W Hughes, E R Wooding, Phys Letters 24A, 70 (1967)	6	6	5 1	0 6	23	760	1 x 10^{16}	Relative intens of 4s5 p lines of Ar I	$T_g = T_{exc} = T_e$		9000	same	8500	Same	Radial + axial
H U Eckert, F L Kelly H N Olsen J Appl Phys 39 1646 (1968)	0 100 60*	7	4		100	760	1 7 x 10^{15}	Stark broadening H_β lines							
P D Scholz T P Anderson JQSRT 8 1411 (1968)	2*	5	4 2	8 x 10^{-2}	25	7 6			10500	Boltzmann graph	8800	Abs. cont. Intens. at 4288 Å			Radial
						76			8300	Boltzmann graph	8300	Abs. cont Intens. at 4259Å			Radial
						380			9400	Boltzmann graph	9100	Abs. cont. Intens. at 4259 Å			Radial
						760			9500	Boltzmann graph	9500	Abs. cont. Intens. at 4259Å			Radial
S V Desai, W H Corcoran JQSRT 8, 1721 (1968) JQSRT 9 1489 (1969)	1 6*	3		7 4 x 10^{-2}	25	760			$T_{exc} = T_e$		9800	Calculated radial ten.p.			Radial
									$T_{exc} = T_e$		9500	space av Boltzmann - Abel			Radial
B S Malone, W H Corcoran, JQSRT 6 443 (1966)	10 1 5*	2 2 5	20	9 x 10^{-2}	33	760			$T_{exc} = T_e$		4500-4800 5700-6000	Boltzmann graph			
Present investigation** discharge region	42 60	2x8***	0 54	0 1 0 36	80	60 650	0 75-1 5x10^{18}	Revised Kramers Unsöld	9000 - 10,000 $T_{exc} = T_e$	Boltzmann graph X-band radiometer			2900-4400	Gas dynamic calculation	
Sonic afterglow region	42 60	2 x 8***	0 54	0 1 0 36	4†	30 150	4x10^{14} 1 75x10^{15}	Kramers-Unsöld, K_a band interferometer	4500 5700	Boltzmann graph			1900-3300	Thermocouple	

* rf power coupled into plasma

** Synopsis of data given in previous figures

*** Centerfed counter wound coil

† Sonic channel diameter

somewhat higher frequency discharges at atmospheric pressure. But the present values differ from those by Eckert, et al.[10] For comparison of the experimental parameters and resultant data of these investigators see Table 3.

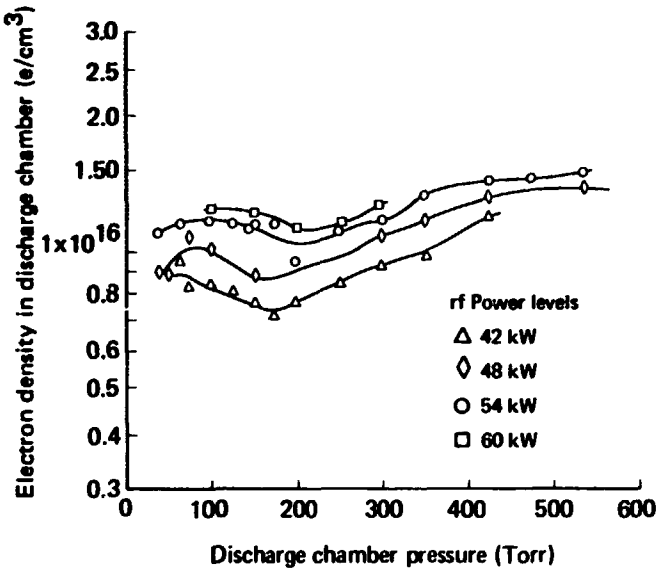

Fig. 8 Electron density in discharge chamber using spectroscopic data and the Kramers-Unsöld formulation

The fact that the optical and microwave methods yield values within 25% over a wide range of plasma conditions is significant, considering that the measurement techniques are based on completely different principles.

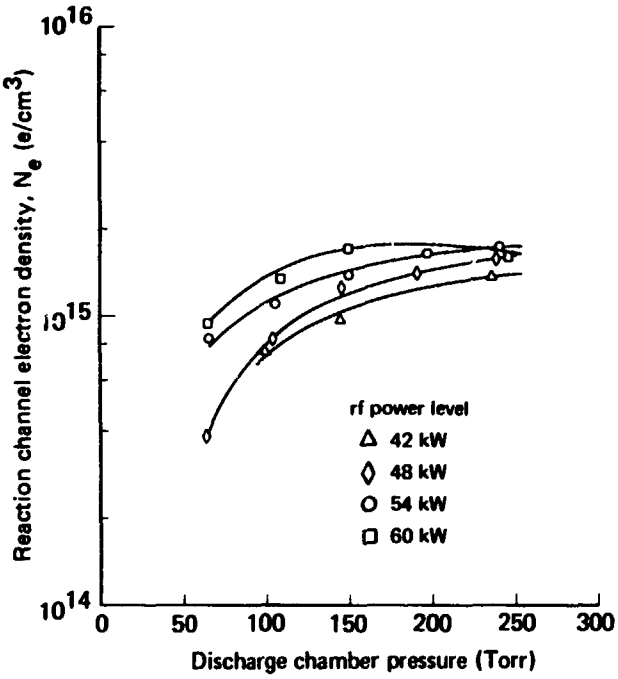

Fig. 9 Reaction channel electron density using interferometer measurements

3.2 Other measurements

The interferometer measurements show the electron density in the channel to be a monotonically increasing function of the discharge pressure over the range considered (Fig. 9). Similar behavior is noted for the electron density as a function of the average reaction channel temperatures determined via thermocouple measurements for 42, 48, and 54 kW, as shown in Fig. 10.

Using the Kramers-Unsöld equation, spectrometric data in the channel yield electron densities that are in good agreement with interferometer measurements extrapolated upstream from the point of measurement in the free jet (Fig. 11a-11d).

Values for the plasma emissivity were obtained by taking the ratio of the effective blackbody radiation and excitation temperatures at various discharge pressures. This procedure assumed that the electron and excitation temperatures were comparable due to the efficient energy exchange between free electrons and the upper bound electronic states. In Fig. 12, the values for the emissivity are compared with calculated ones obtained from a slab plasma model (Appendix A). In this calculation the spectrometrically determined values for the excitation temperatures were used for the electron temperatures. Agreement between the calculated and measured emissivities (Fig. 12) indicates that the excitation and electron temperatures approximate

each other in the discharge. The electron densities from the emissivity calculations shown in Fig. 12 are compared with the optical measurements. The computed values of the electron density are higher than the measured values. Using the measured electron density directly in the emissivity program did not significantly alter the overall emissivity results for the range of discharge pressures considered.

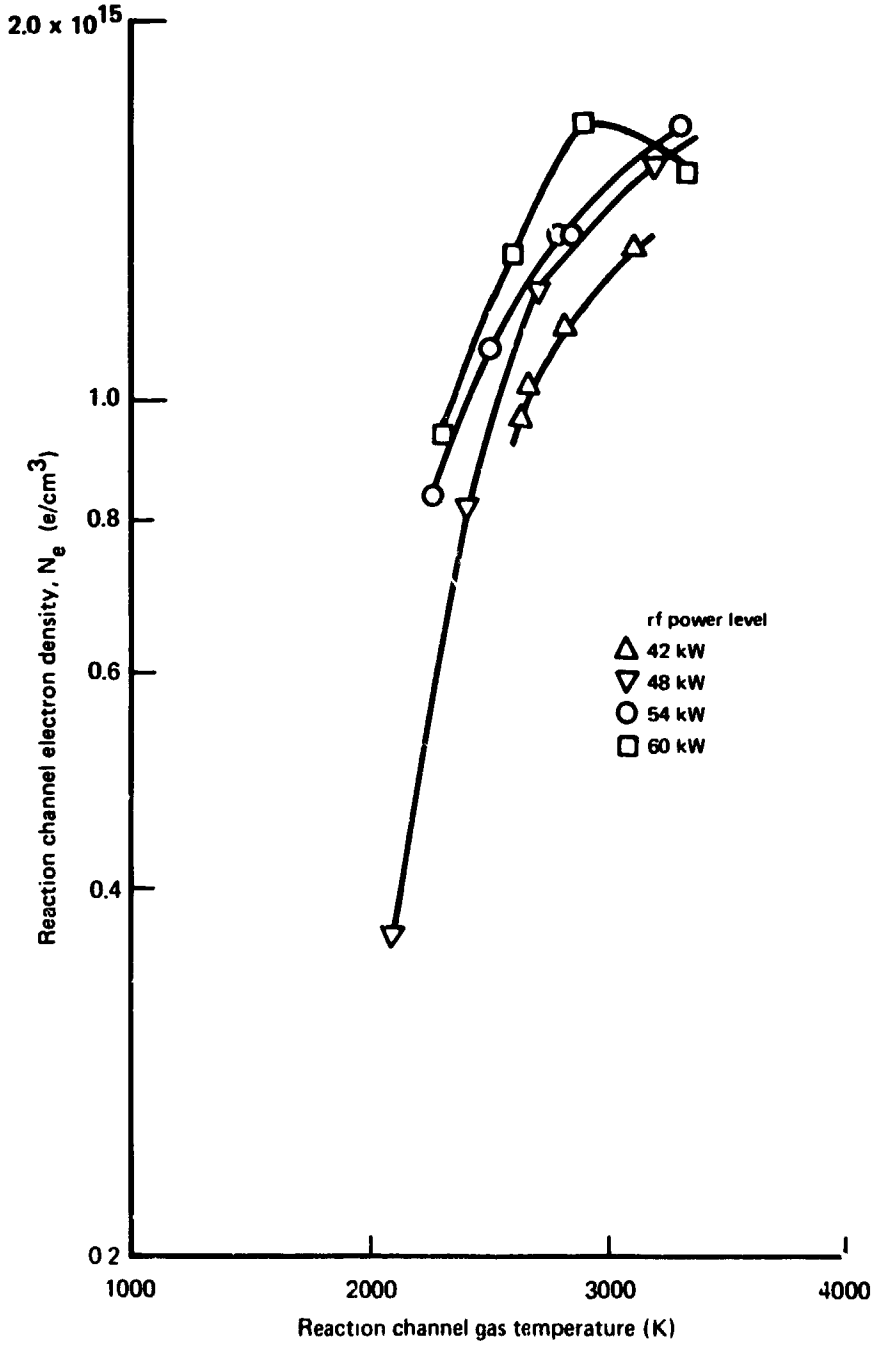

Fig. 10 Reaction channel electron density as a function of channel gas temperature. Electron density measured with Ka-band interferometer. Gas temperature measured with a tungsten-rhenium thermocouple placed in the centerline of the channel

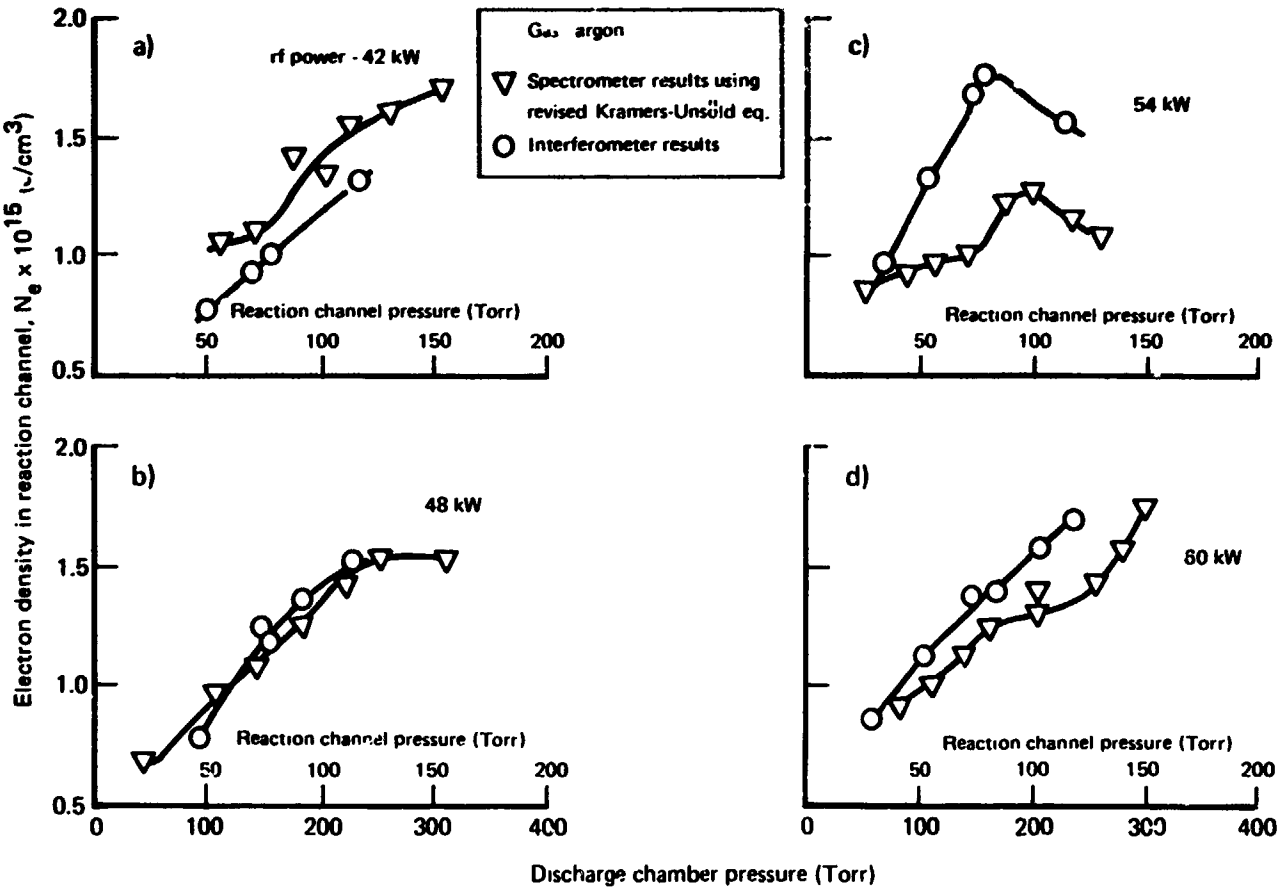

FIG. 11 Comparison of spectrometer and interferometer data in reaction channel

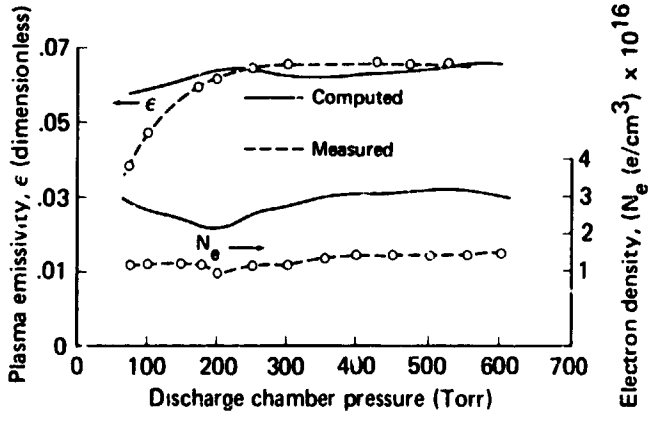

Fig. 12 Plasma emissivity and electron density as a function of discharge pressure rf power - 54 kW

4 Discussion

The state of the plasma in the discharge and the sonic afterglow (reaction channel) regions, as determined from the preceding measurements are summarized below. Additional discussion of thermocouple results as well as supplementary optical and gas dynamic considerations are included.

(a) From the electron densities alone, measured by the spectrometer in the discharge and extrapolated from the radiometer data, there appear to be more electrons present in the discharge than would be predicted by the Saha equation; e.g., an argon plasma under total thermodynamic equilibrium (TE) conditions at 9000 K has an electron density of 1.8 to 5.1 x 10^{15} e/cm^3 for pressures of 100-700 Torr. These values are considerably less than the spectrometrically measured values (Fig. 8). Thus the plasma is not in total TE over the range of discharge pressures considered. However, a two-temperature "bottleneck level" plasma model satisfactorily explains the experimental observations. This concept will be elaborated in a later section.

(b) Trace quantities of nitrogen gas (0.042 and 0.084 mole %) were injected into the argon to obtain N_2 rotational temperatures in the channel by using the rotational lines of N_2 and N_2^+. Specifically, the rotational lines of the R branches of the $C^3\Pi_u - B^3\Pi_g$ 0-1 second positive band of N_2 were observed spectrometrically in the channel when the power was 54 kW and chamber pressure 139 Torr. Uninverted scans of the unresolved triplets in the R branches (J = 32 to J = 45) were treated as described by Robinson[22]. The resulting rotational temperature was calculated to be 1950 K.

In addition, the rotational lines of the R branch of the $B^2\Sigma_u^+ - X^2\Sigma_g^+$ 0-0 first negative band of N_2^+ were observed spectrometrically in the chamber at 48 kW power and 124 Torr chamber pressure. Nitrogen gas was injected into the argon at 0.57 mole %. An uninverted scan was made and treated as described in Appendix B. Most of the lines from J = 2 to J = 48 were visible but weak when compared with the intense continuum of argon. The rotational temperatures were estimated to be at least 2100 K.

(c) Calculations of the gas temperature based on gas dynamic considerations indicate that the approximate spatially-averaged value of the temperature in the discharge chamber varies between 2900-4400 K for chamber pressures between 50-600 Torr (Fig. 13). For this calculation an isentropic flow from the discharge chamber was assumed with negligible wall loss. Also, the flow velocity was assumed to be sonic at the discharge chamber exit with the mass of the gas being carried by the heavy gas particles.

(d) Measurements with tungsten-rhenium thermocouples in the channel for mass flows of 0.1-0.36 g/sec and 42-60 kW input power indicated that the gas temperatures ranged between 1900-3320 K (Fig. 14)[3]. The mean gas temperature calculated for the discharge and the values extrapolated from the thermocouple data, i.e., 2500-4400 K, are in agreement if isentropic expansion is assumed. The

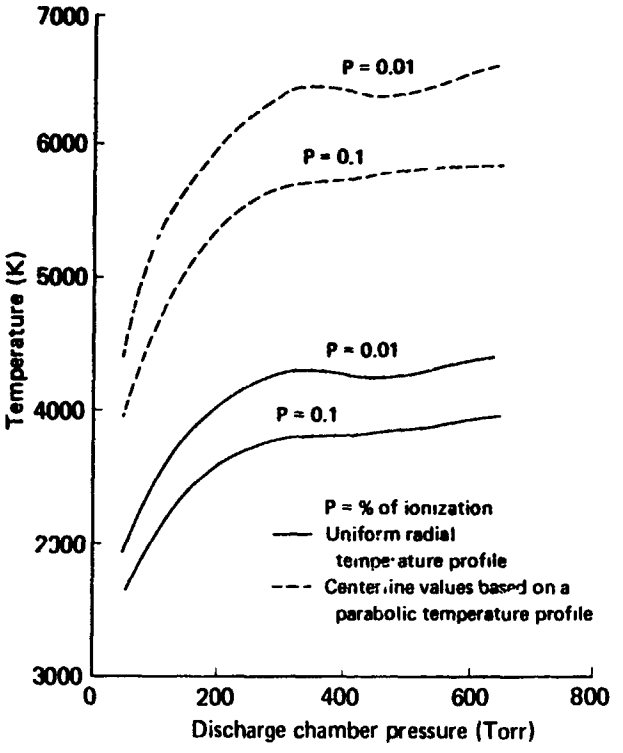

Fig. 13 Estimate of peak discharge chamber gas temperature (calculated from gas dynamics)

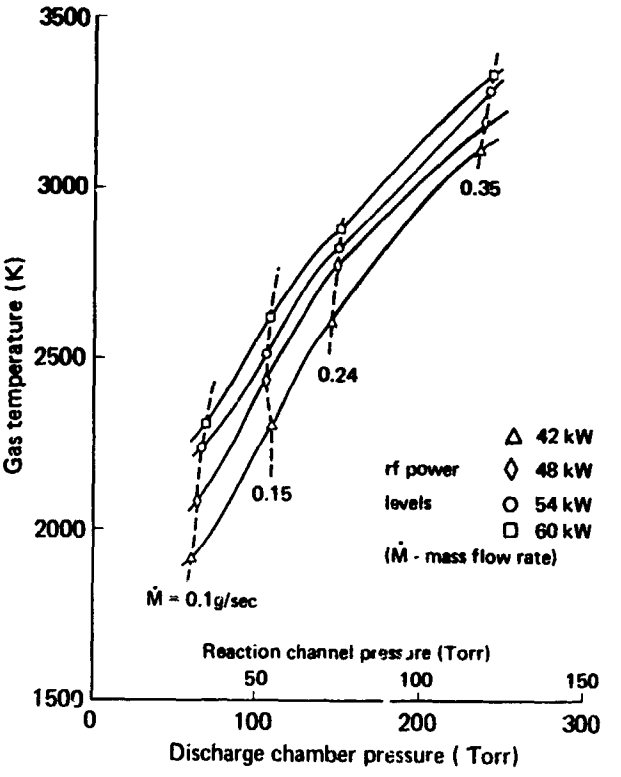

Fig. 14 Gas temperatures in reaction channel

thermocouple measurements as well as the calculated mean temperatures noted in c, are a conservative lower limit to the true centerline temperatures. Comparison of all of these values to the spectrometrically measured excitation and rotational temperatures in the discharge chamber and the reaction channel shows that TE probably does not exist in either place.

(e) As was noted in Section 3, the optical and interferometer data from the channel yield closely correlated values for the electron density in the channel (Figs. 11a - 11d). The channel electron density varies from 0.6 to 1.75 x 10^{15} e/cm^3 for the range of discharge conditions considered.

(f) Optical measurements in the discharge chamber at 54 kW indicate that the excitation temperature decreases rapidly from 10,000 K between 100-200 Torr and then attains a steady value around 8000 K for the higher pressures (> 300 Torr). Similar behavior has been noted at the other power levels. The measured values of the excitation temperature are in agreement with those found by Scholz and Anderson[23] at 75 and 380 Torr for a flowing argon rf plasma exhibiting LTE (Fig. 15). Their discharge was operated at lower mass flow rates and power levels (see Table 3). The excitation temperatures here were obtained from a Boltzmann graph using nine line intensities; Scholz and Anderson used four lines. Their equilibrium temperature was obtained from the absolute continuum intensity at 4259 Å.

(g) The excitation temperatures in the reaction channel are found to be a weakly decreasing function of pressure (for all levels of rf excitation) with final values averaging 4500 K (Table 2). As in the discharge chamber, the ratio of excitation temperature to gas temperature (obtained from a thermocouple) is approximately two and remains essentially invariant for the entire range of chamber pressures and rf excitation levels, again indicating that the plasma is in a two temperature state.

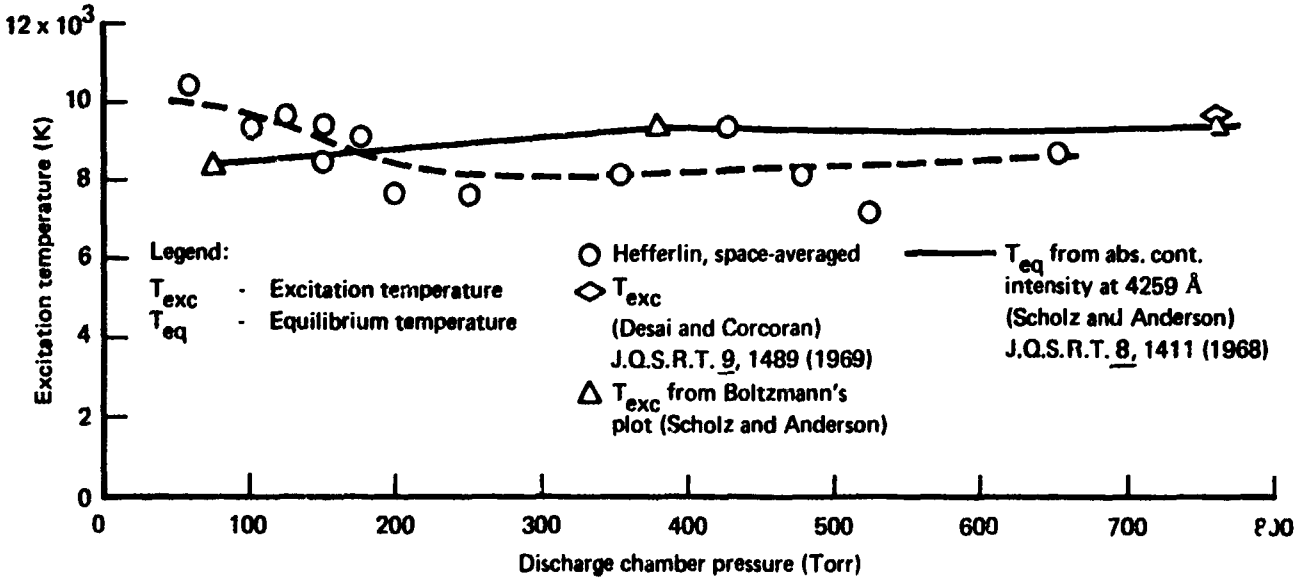

Fig. 15 Spectroscopic measurements in rf argon plasma (54kW - input power)

4.1 Two-temperature bottleneck-level plasma model

The foregoing experimental observations and analytical considerations suggest that a consistent description of the plasma both in the discharge and the reaction channel requires the two-temperature bottleneck-level plasma model suggested in a. This model, specifies explicitly that excited levels above some critical energy level are populated in equilibrium with the free electrons (at temperature T_e). The gas is at lower temperature, T_g. The critical level can be found using the standard criteria for LTE stated by Griem[24] for hydrogen and hydrogen-like atoms or ions. Since the energy level diagram of argon is similar to that of hydrogen, these criteria are applicable to the present discussion.

First, the LTE criterion for the upper excited states is applied (Griem, Eq. 6-55). Using the spectrometric results for the discharge chamber of $N_e \leqslant 1 \times 10^{16}$ e/cm^3 and $T \cong 8000$ K the critical level for LTE is shown to be at the principal quantum number $n \cong 1.5$. Since this value is inadmissible as a principal quantum number but the next higher integer is, it is concluded that all hydrogen-like levels $n \geqslant 2$ are in LTE. Applying this result to argon requires that all levels from the first excited state on are in LTE. Similarly applying the Griem criterion to the channel region for $N_e \cong 3 \times 10^{15}$ e/cm^3 and $T \cong 4500$ K gives the critical level as $n \cong 2.0$ Thus, the first excited level of argon, being somewhat higher than that for hydrogen, is in LTE with everything above it.

For the ground state the existence of LTE must be determined separately because of greater deviations from hydrogenic behavior. For these cases a modified criterion for LTE may be used (Griem, Eq. 6-60) which requires that the ground level be populated ten times more often by collisions than by radiation. Applying this relationship indicates that the electron density is not sufficient to guarantee an LTE population for the argon ground level. This observation supports the conclusions obtained from the previous LTE criterion above. The fact that the Griem criterion is satisfied for $n \geqslant 2$ in both the discharge chamber and the reaction channel "justifies" the interpretation of the slope of the Boltzmann graph as an excitation temperature. Finally, the hypothesis of LTE is also supported by the close agreement of the electron and the excitation temperatures as obtained from the spectrometric and radiometric data and the emissivity calculations.

5 Summary

The plasma in the rf discharge and the sonic afterglow regions appears to be in a two-temperature state. Comparison of the electron densities obtained from the Kramers-Unsöld formulation with those obtained from an equilibrium calculation indicates that the excitation and the gas (heavy particle) temperatures are not equal. However, the excitation and electron temperatures are approximately equal in the discharge itself, averaging 8000 K over the pressures and rf power levels considered. The gas temperatures calculated from gas dynamic considerations and extrapolated from thermocouple data average 4400 K. In the sonic afterglow region the corresponding values of the excitation and heavy particle temperatures are almost 50% less than those measured in the discharge chamber. Independent microwave interferometer measurements of the electron density confirm the Kramers-Unsöld values obtained in the reaction channel. Optical thinness was established in both the discharge and the sonic afterglow regions. Using the standard tests for LTE, the plasma is shown in both regions to be in LTE in all but the ground level.

Acknowledgement

The authors wish to acknowledge the valuable suggestions and comments of Drs. J.M. Madson, J.H. Mullen, and T.C. Peng in connection with this investigation.

6 References

1. F.T. Smith, Kinetic Processes in Gases and Plasmas, (A.R. Hochstim, ed.), (Academic Press, New York and London, 1969) p. 257–280.
2. E.E. Ferguson, Advances in Electronics and Electron Physics, (L. Marton, ed.), (Academic Press, New York and London, 1968), Vol. 24, p. 1–50.
3. J.H. Mullen, J.M. Madson, L.N. Medgyesi-Mitschang, T.C. Peng, and P.M. Doane, Rev. Sci. Instr. 41, 1746 (1970).
4. K.S. Knol, Phillips Research Rpt. 6, 288 (1951).
5. M.A. Easley and W.W. Mumford, J. Appl. Phys. 22, 846 (1951).
6. L.E. Brewer and W.K. McGregor, Proc. 6th Intern. Conf. on Ioniz. Phenomena in Gases, (Paris), 1, paper II-27 (1963).
7. A.N. Dellis, Rpt. A.E.R.E. GP/R2265, U.K. Atomic Energy Authority (1957).
8. G.A. Harding, A.Dellis, A.Gibson, B.Jones, D. Lees, R. McWhirter, S.Ramsden, S Ward, "Diagnostic Techniques Used in Controlled Thermonuclear Research at Harwell," Proc. 2nd U.N. Conf. Peaceful Uses of Atomic Energy (Geneva) 32, 365 (1958).
9. T.B. Reed, J. Appl. Phys. 32, 821 (1961).
10. H.V. Eckert, F.L. Kelly and H.N. Olsen, J. Appl. Phys. 39, 1846 (1968).
11. J.H. Mullen and E.A. Theby, Patent Disclosure, MDC File No. 70–112, "High Temperature Centerfed Radio Frequency Plasma Heating Torch." (Nov. 1971)
12. R.H. Dicke, Rev. Sci. Instr. 17, 268 (1946).
13. D.B. Harris, Microwave Journal 3, 41, 47 (1960).
14. P.D. Strum, PROC. IRE 48, 43 (1958).
15. E.A. Ohm and W.W. Snell, Bell Syst. Tech. J. 42, 2047 (1963).
16. R. Hefferlin, Progress in High Temperature Physics and Chemistry, (C.A. Rouse, ed.) (Pergamon Press, New York, 1969), Vol. 3, Chap. 2.
17. J. Richter, Plasma Diagnostics (Lochte Holtgreven, ed.), (North-Holland Press, Amsterdam, 1968) Chap. 1.
18. H.N. Olsen, Phys. Rev. 124, 1703 (1961).
19. W.L. Wiese, M.W. Smith and B.M. Miles, Atomic Transition Probabilities, National Standard Reference Data Service, National Bureau of Standards 22, (Oct. 1969).
20. D.W. Hughes and E.R. Wooding, Phys. Letters 24A, 70 (1967)
21. V.M. Goldfarb and S.V. Dresvin, High Temperature, (Russian) 3, 303 (1965).
22. D.Robinson, "Spectroscopic Measurements of Heavy Particle Temperatures," Northrop Space Laboratory Report NSL 63–191 (Sept. 1963).
23. P.D. Scholz and T.P. Anderson, JQSRT 8, 1411 (1968).
24. H.R. Griem, Plasma Spectroscopy (McGraw Hill Book Co., New York, 1964) Chap. 6.

7 Appendix A - Emissivity calculation

To relate the effective blackbody radiation temperature of a plasma source to the electron temperature, the plasma emissivity must be known. The pertinent expressions for the plasma emissivity are derived below.

If full reciprocity exists in the propagation characteristics of the medium, then the emissivity and absorptivity may be used interchangeably as a consequence of Kirchhoff's law of radiation. Mathematically the emissivity (or absorptivity) may be stated in the usual notation as:[1]

$$\epsilon = A = \frac{\int_V \mathrm{Re}\,(\vec{J} \cdot \vec{E}^*)\, dv}{\int_S \mathrm{Re}\,(\vec{E}_o \times \vec{H}_o^*)\, ds} \qquad \text{(A-1)}$$

where V and S are the volume and projected area of the sample being illuminated by an electromagnetic test wave, composed of electric and magnetic field intensities, $\vec{E}_o$ and $\vec{H}_o$, respectively. The quantities $\vec{J}$ and $\vec{E}$ are the current density and electric field intensity within the sample. Alternately the emissivity may be formulated as

$$\epsilon = A = 1 - R - T \qquad \text{(A-2)}$$

where T and R are the power transmission and reflection coefficients, respectively. Specific expressions for R and T will be derived for a slab plasma.

For the case where the plasma can be considered a plane, effectively homogeneous slab, a plane wave analysis[1], assuming incoherence in the reflected waves within the slab, yields a reflection coefficient, ρ, as

$$\rho = \frac{\left(\frac{\eta_o}{\eta_1} - \sqrt{K_3}\right) \cos k_2 \ell + j \left(\sqrt{\frac{K_3}{K_2}}\frac{\eta_o}{\eta_1} - \sqrt{K_2}\right) \sin k_2 \ell}{\left(\frac{\eta_o}{\eta_1} + \sqrt{K_3}\right) \cos k_2 \ell + j \left(\sqrt{\frac{K_3}{K_2}}\frac{\eta_o}{\eta_1} + \sqrt{K_2}\right) \sin k_2 \ell}; \qquad \text{(A-3)}$$

$$\sqrt{K_2} \equiv \mu_2 - j\chi_2; \quad \sqrt{K_3} \equiv \mu_3 - j\chi_3; \quad k_2 = \frac{\omega}{C}\sqrt{K_2}\,.$$

η_1 is the wave impedance of the medium outside of layers 2 and 3, $\eta_o = 377\ \Omega$ (the free space impedance), and K_2 and K_3 are the complex dielectric constants of layers 2 and 3, representing in the present analysis the water layer in the discharge jacket and the plasma, respectively. The power reflection coefficient is defined by $R \equiv |\rho|^2$ where ρ is given in Eq. (A-3).

Measurements indicate that the plasma attenuation in the present case exceeds 50 dB; thus $T \cong 0$. The defining equations for the plasma (layer 3) are:

$$\left.\begin{matrix}\mu_3 \\ \chi_3\end{matrix}\right\} = \left\{ \pm \frac{1}{2} \left(1 - \frac{\omega_p^2}{\omega^2 + \nu^2}\right) + \frac{1}{2} \left[\left(1 - \frac{\omega_p^2}{\omega^2 + \nu^2}\right)^2 + \left(\frac{\omega_p^2}{\omega^2 + \nu^2} \frac{\nu}{\omega}\right)^2\right]^{1/2} \right\}^{1/2} \quad \text{(A-4)}$$

The collision frequency for electron-ion interactions (Coulomb interactions), ν_{ei}, is given using the Appleton-Bray formulation[2] as

$$\nu_{ei} = \frac{8}{3}\left(\frac{\pi}{m_e}\right)^{1/2} N_e \frac{e^4}{(2kT_e)^{3/2}} \ln\left[\frac{k^3 T_e^3}{\pi N_e e^6}\right] \quad \text{(A-5)}$$

(assuming that $N_i = N_e$). The collision frequency for the less dominant electron-neutral interactions is given by

$$\nu_{ea} = \frac{N_e}{\rho} \sigma_{ea} \left(\frac{8kTe}{\pi m_e}\right)^{1/2},$$

where the collision cross section, σ_{ea}, is given as[3]

$$\sigma_{ea} = \begin{cases} [-0.35 + 0.775\,(10^{-4})\,T_e]\ 10^{-16}; \\ \text{for } T_e > 10^4 K \\ [0.39 - 0.551\,(10^{-4})\,T_e \\ + 0.595\,(10^{-8})\,T_e^2\,]\ 10^{-16}; \\ \text{for } T_e \leqslant 10^4 K. \end{cases} \quad \text{(A-6)}$$

An additional relationship can be derived for N_e in terms of the discharge chamber pressure and mass flow rate giving

$$N_e = \frac{0.962 \times 10^{19} P_T}{\left[\frac{0.7545}{p} = 10^{-4}\left(\frac{P_T}{\dot{M}}\right)^2 \frac{M_o}{1+p} + T_e\right]} \quad \text{(A-7)}$$

Five assumptions were made in deriving Eq.(A-7): 1) isentropic flow from the discharge chamber, 2) sonic flow at the exit, 3) applicability of the perfect gas law, 4) mass of the gas carried by the heavy particles, and 5) no significant temperature gradient in the chamber.

The foregoing set of equations defining the plasma emissivity for the slab case may be rearranged for computer calculations so that the electron temperature and the percentage of ionization may be retained as parameters in the calculations. A typical result from these calculations is given in Fig. 12, indicating reasonable agreement with the experimental data from the radiometer and spectrometer.

References

1. *M.A. Heald and C.B. Wharton, Plasma Diagnostics with Microwaves, (John Wiley, New York, 1965), p. 128-130, 270-271.*

2. *J.P. Appleton and K.N.C. Bray, Fluid Mech. 20, 659 (1964).*

3. *I.P. Shkarofsky, M.P. Bachynski, T.W. Johnston, Planetary Space Sci. 6, 24 (1961).*

Symbols used in Appendix A:

N_i = ion density (ions/cm^3)
N_e = electron density (e/cm^3)
ω_p = plasma frequency ($\omega_p = 5.63 \times 10^4 \sqrt{N_e}$)
f = frequency of the EM wave (Hz)
ν = $\nu_{ea} + \nu_{ei}$ = effective collision frequency
T_e = electron temperature (K)
P_T = discharge chamber pressure (Torr)
$\dot{M}$ = mass flow rate (g/sec)
p = fraction of ionization
M_o = atomic weight (g)
ℓ = thickness of layer 2
c,e,m_e,k = velocity of light (cm/sec); electron charge (e.s.u.), electron mass (g), Boltzmann constant

8 Appendix B - Determination of rotational temperatures*

The electron translational temperature, in laboratory plasmas, usually determines the excitation temperature of the heavy particle energy levels. It is of interest to learn that the heavy particle translational temperature can determine the rotational temperature of a molecular species. Thence molecular spectroscopy might be a tool for finding this otherwise evasive property. For this reason, the present determination of a molecular rotational temperature was undertaken.

The plasma jet which produced these spectra was being operated in the laminar, subsonic mode, and there was reason to hope that local thermodynamic equilibrium existed. The 0-0, 1-1, and 2-2 bands of N_2^+ (region 3700-3900 Å) were well developed and at least the 0-1 band (region 4200-4300 Å) was visible. All of these bands belong to the $B^2\Sigma$-$X^2\Sigma$ system, which is called a "negative system" (in contrast to the "positive systems" which are emitted by neutral N_2) because of where it appears in a common discharge tube. The appearance of molecular nitrogen is due to the seeding of the plasma jet operating gas, argon, by a 50% (by weight) aqueous solution of $Mn(NO_3)_2$ in such an amount that there were 12.9 nitrogen atoms per million argon atoms. The spectrometer saw light from a diameter through the plume 1 in. downstream of the exhaust plume.

8.1 Theory

The relative intensities of entire bands emitted by molecules in an optically thin gas in local thermodynamic equilibrium (LTE) are proportional to the populations of the upper rotational levels, given by the equation:

$$n(v') = n(0)e^{-G(v')hc/kT}, \qquad \text{(B-1)}$$

(Ref. 1) in which

$$G(v') = \omega_e'(v' + 1/2) + \omega_e' x_e'(v' + 1/2)^2 + \omega_e' y_e'(v' + 1/2)^3 \qquad \text{(B-2)}$$

and

v' = vibrational quantum number of upper levels,
T = vibrational excitation temperature,

ω_e', $\omega_e' x_e'$, $\omega_e' y_e'$ are numbers tabulated by Herzberg (Ref. 1).

The relative intensities of the rotational lines in an optically thin gas in LTE within a given band and branch are given by

$$I = C \frac{1}{\lambda^4}(J' + J'' + 1)e^{-B_v' J'(J' + 1)hc/kT}, \qquad \text{(B-3)}$$

**Material in this appendix is taken from an internal McDonnell Douglas Report entitled "A Method of Obtaining Rotational Excitational Temperature from Spectroscopic Observation of a Plasma" by R.J. Checkley and R.A. Hefferlin (Dec. 1967).*

The measurements in this appendix were made in an arc plasma source, that was entirely different from the rf discharge described earlier. The method of analysis is the same as described in Section 4.

for which

T = rotational excitation temperature,
J′ = rotational quantum number of the upper level,
J″ = rotational quantum number of the lower level.

The selection rules are such that for a P branch

$$(J' + J'' + 1) = (J'' - 1) + (J'' + 1) = 2J'', \qquad \text{(B-4)}$$

and for an R branch

$$(J' + J'' + 1) = (J'' + 1) + (J'' + 1) = 2J'' + 2. \qquad \text{(B-5)}$$

Also

$$B_v' = B_e - \alpha_e (v' + 1/2), \qquad \text{(B-6)}$$

where v′ is the vibrational quantum number of all the upper rotational levels and B_e and α_e are molecular constants again tabulated by Herzberg.

Algebraic manipulation of Eq. (B-3) yields (base 10)

$$\log \frac{I\lambda^4}{(J' + J'' + 1)} = \log C - \frac{B_v' J' (J' + 1) hc}{2.3 kT}. \qquad \text{(B-7)}$$

If the entire left hand side is plotted on a y axis, and J′ (J′ + 1) is plotted on an x axis, the points plotted should fall along a straight line with

$$\text{Slope} = -\frac{B_v' hc}{2.3 kT} \qquad \text{(B-8)}$$

Solution of this equation then gives the rotational excitation temperature (correction must be made for the alternation of intensities which results from the influence of nuclear spin; otherwise two parallel lines will appear on the temperature graph due to the fact that every other line is twice as bright as its neighbors.)

In the particular case at hand, the quantum number J″ is replaced, by molecular spectroscopists, with the quantum number K″, or, identically, with K. The quantum number J′ could likewise be replaced by K′; however it is more common to use the selection rules, Eqs. (B-4) and (B-5), to express J′ in terms of K[2,3]. We retain the J′ and J″ notation, however, in this report.

The procedure of obtaining the rotational temperature presupposes that one can identify the rotational quantum numbers of the individual lines. The difficult job of accomplishing this identification will be described in the following section, as will the explanation of a correction applied due to blending of lines.

8.2 Procedure

At low temperatures (e.g., room temperature) the (absorption) spectrum of the negative $B^2\Sigma$-$X^2\Sigma$ bands of the N_2^+ molecular ion exhibits clear separation of the separate bands, thus leaving only the problem of separating lines from the various branches of one band from one another.[1]
At higher temperatures the emission lines of the different bands lie among each other, causing a much more difficult problem.[4] In the spectrum under study, the lines from various bands were overlapped to the extent that attempts to assign rotational quantum numbers, branch numbers, and vibrational quantum numbers by comparison with a published spectrum[4] were completely unsuccessful.

A model of the spectrum was therefore constructed from basic molecular data and from assumed source conditions. Wavelengths of the first 150 lines from the P and R branches of the 0-0, 1-1, 2-2, and 3-3 bands were calculated from molecular constants given by Herzberg. Relative intensities of lines in selected wavelength regions

were calculated by multiplying (a) the exponential term* of Eq. (B-1), (b) the parenthesis term and the exponential term* of Eq. (B-3), and (c) the intensity alternating factor due to nuclear spin. A histogram was constructed by summing all these intensities in 0.8 Å increments of wavelength.+ This histogram strikingly resembled the strip chart spectra. Those few of the histogram peaks which were due primarily to a single line of a single branch of one of the bands then allowed the assignment of rotational quantum numbers to the corresponding spectrum features. All of these features were in the 0-0 band. The assignment of rotational quantum numbers was checked by plotting a Fortrat parabola (quantum number vs wave number)[1]; the wave number minimum of the parabola was found algebraically to fall at the 0-0 band head. These considerations also allowed assignment of rotational quantum numbers in the R branch of the 0-0 band to a very regular series of lines far to the blue side of all the band heads and blended lines ($J'' = 70$ and beyond). It was next necessary to measure the intensities of as many lines as possible. There would not be many because the number of spectrum features due primarily to a single line - according to comparison with the histogram - was small. And bending was to be expected even in the features now identified with $J'' > 70$.[4]

The intensities, I, were obtained by multiplying the heights of the isolated features (top of strip chart = 100) by their widths (full width at half maximum in mm) and by the spectrograph calibration obtained with a tungsten standard lamp. These intensities were then dealt with in two ways:

1. They were multiplied by λ^4, and by 2 if J'' was odd; they were divided by $2(J''+1)$ if in the R branch and by $2J''$ if in the P branch; and the common logarithm was taken. The results of these operations were plotted against $J'(J'+1)$, as required by Eq. (B-6). A typical calculation appears in Table B-1. The plot is shown in Fig B-1; the slope of the selected straight line is -3.36×10^{-4}.

2. They were multiplied by λ^4 and by the correction factors** given in (Ref. 4); they were divided by $2(J''+1)$ if in the R branch and by $2J''$ if in the P branch; the common logarithm was taken. The results of these operations were plotted against $J'(J'+1)$, as required by Eq. (B-6). A typical calculation appears in Table B-1. The plot is shown in Fig. B-2; the slope of the selected straight line is -3.84×10^{-4}.

8.3 Results

The use of Eq. (B-7) made it possible to find the rotational excitational temperatures for the two methods once the slopes of the Boltzmann plots (Figs. B-1 and B-2) were known. Respectively, these temperatures were 4300 K and 3750 K. Due to the subjective nature of the selection of the lines in Figs. B-1 and B-2, these numbers are considered to mean that the correct value is 4000 K $\pm$300 K. This rotational excitational temperature is, of course, an average through the plume of the plasma jet.

8.4 Conclusions

The rather large scatter of the points in Figs. B-1 and B-2 is probably due (a) to fluctuations in the source and (b) to the presence of one or two atomic spectrum lines.

The histogram, which makes quantum number identification possible, does not depend upon having presupposed the correct temperature in the exponential terms of Eq. (B-1) and (B-3).

It was assumed that T was 12,500 K

+Our instrument bandpass

***Due to the low temperature obtained in the first method the correction factors of Ref. (4) were linearly extrapolated to 4000 K. Linear interpolation was considered satisfactory as far as the quantum numbers, J'', were concerned.*

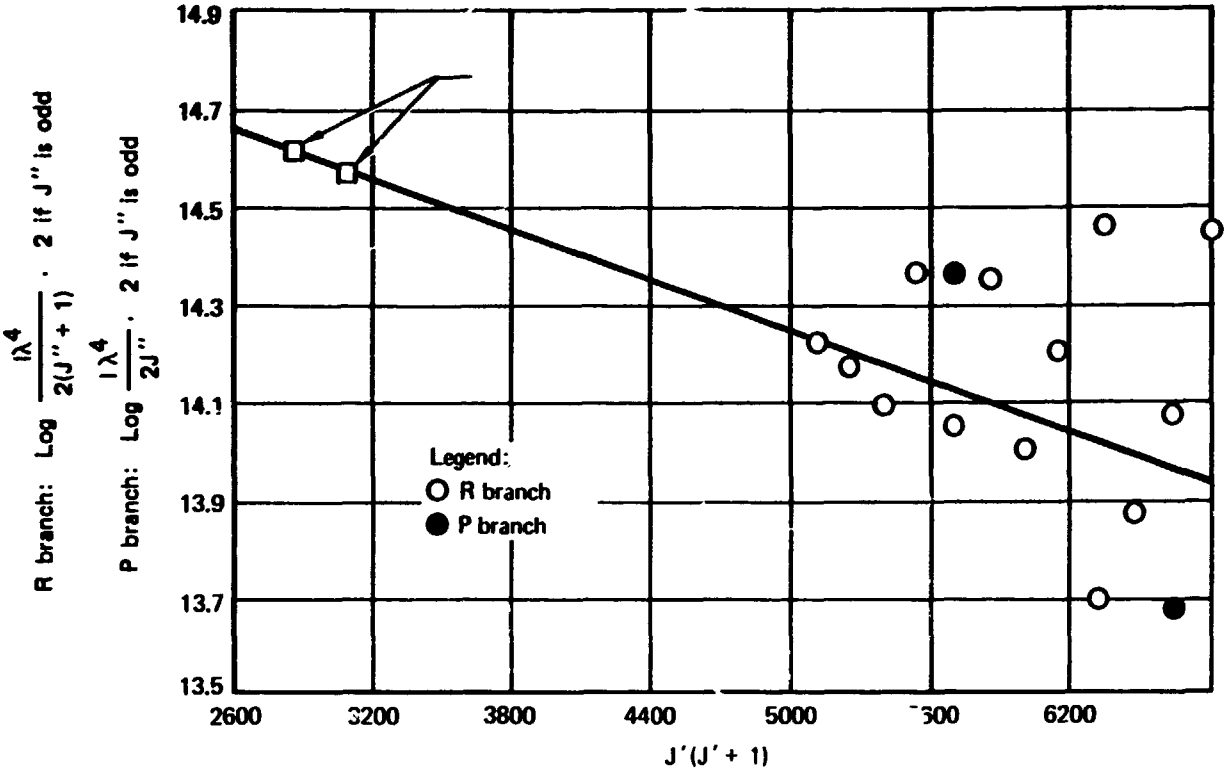

Fig. B-1 Boltzmann plot using Eq. B-6

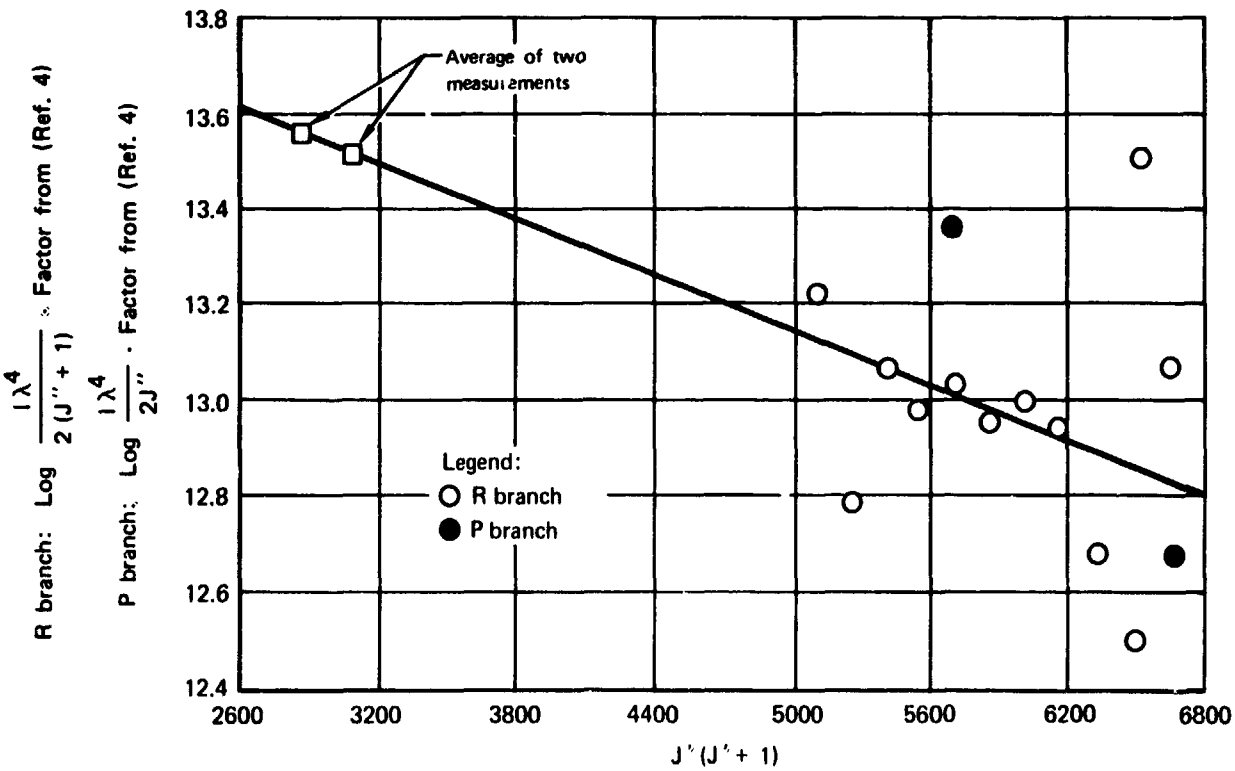

Fig. B-2 Boltzmann plot using correction factor of Ref. 4

Table B-I
Typical calculations
(Using N_2^+ 0-0 band, rotational line J" = 79, in R branch)

Quantity or operation	Numerical calculation	
	Using Eq. (B-6)	Using correction factor of Ref. 4
(1) Line recording area (top of chart = 100; FWHM in mm)	13.5	13.5
(2) Instrument response function (relative)	2.25	2.25
(3) Wavelength (in A)	3,725	3,725
(4) λ^4	1.92×10^{14}	1.92×10^{14}
(5) Multiple by 2 if J" is odd	2	
(6) Correction factor of (Ref. 4)		0.88
(7) Divide by 2(J" + 1) if in R branch, by 2J" if in P branch	160	160
(8) Product of (1), (2), (4), (5), or (6), divided by (7)	7.2×10^{13}	3.2×10^{12}
(9) Logarithm (base 10), which is plotted on "y" axis of Fig. B-1 or Fig. B-2	13.862	12.505
(10) J'	80	80
(11) J'(J' + 1), which is plotted on "x" axis of Fig. B-1 or Fig. B-2	6,480	6,480

Although two methods were used to reduce the raw data, one of which assumed that even those features finally isolated were still blended, these two methods gave substantially the same final result.

8.5 References

1. *Gerhard Herzberg, Molecular Spectra and Molecular Structure. I Spectra of Diatomic Molecules, (D. Van Nostrand Co., Inc., New York, 1950).*
2. *R.A. Hefferlin, "Diagnostics in Field-Free Plasmas with Medium-Dispersion Optical-Spectrographic and Source-Monitoring Equipment," Progress in High Temperature Physics, Chemistry and Technology, Vol. 3, Pergamon Press, New York, (1969).*
3. *R.A. Hefferlin, "The Measurement of Absolute Spectral Line Intensities," McDonnell Report B032, (December 1964).*
4. *Lothar Klein, H.J. Babrov, "Spectroscopic Studies of Argon and Nitrogen Plasmas at Reduced Pressure. Temperature Distributions in Plasmajets and Wall Stabilized Arcs." Warner and Swasey Report ARL 64 - (December 1964).*